⌘ *Author's Choice*

THE JOURNAL OF BIOLOGICAL CHEMISTRY VOL. 284, NO. 15, pp. 10056–10066, April 10, 2009
© 2009 by The American Society for Biochemistry and Molecular Biology, Inc. Printed in the U.S.A.

Structure and Functional Properties of *Bacillus subtilis* Endospore Biogenesis Factor StoA*[S]

Received for publication, December 19, 2008 Published, JBC Papers in Press, January 13, 2009, DOI 10.1074/jbc.M809566200

Allister Crow[‡1], Yiming Liu[§1], Mirja Carlsson Möller[§], Nick E. Le Brun[‡2], and Lars Hederstedt[§3]

From the [‡]Centre for Molecular and Structural Biochemistry, School of Chemical Sciences and Pharmacy, University of East Anglia, Norwich NR4 7TJ, United Kingdom and the [§]Department of Cell and Organism Biology, Lund University, Lund SE-22362, Sweden

Bacillus subtilis **StoA is an extracytoplasmic thiol-disulfide oxidoreductase (TDOR) important for the synthesis of the endospore peptidoglycan cortex protective layer. Here we demonstrate that StoA is membrane-associated in *B. subtilis* and report the crystal structure of the soluble protein lacking its membrane anchor. This showed that StoA adopts a thioredoxin-like fold with N-terminal and internal additions that are characteristic of extracytoplasmic TDORs. The C*XX*C active site of the crystallized protein was found to be in a mixture of oxidized and reduced states, illustrating that there is little conformational variation between redox states. The midpoint reduction potential was determined as −248 mV *versus* normal hydrogen electrode at pH 7 consistent with StoA fulfilling a reductive role in endospore biogenesis. pK_a values of the active site cysteines, Cys-65 and Cys-68, were determined to be 5.5 and 7.8. Although Cys-68 is buried within the structure, both cysteines were found to be accessible to cysteine-specific alkylating reagents. *In vivo* studies of site-directed variants of StoA revealed that the active site cysteines are functionally important, as is Glu-71, which lies close to the active site and is conserved in many reducing extracytoplasmic TDORs. The structure and biophysical properties of StoA are very similar to those of ResA, a *B. subtilis* extracytoplasmic TDOR involved in cytochrome *c* maturation, raising important general questions about how these similar but non-redundant proteins achieve specificity. A detailed comparison of the two proteins demonstrates that relatively subtle differences, largely located around the active sites of the proteins, are sufficient to confer specificity.**

Bacteria of the genera *Bacillus* and *Clostridium* can form endospores in response to nutrient starvation. The endospore, which is a dormant and very resistant state of the bacterium, can germinate back into a vegetative cell once nutrients become available again. Different layers help to protect the endospore: the dehydrated core, corresponding to the cytoplasm and containing the genome, is surrounded by a peptidoglycan layer, the cortex, which is required for extreme heat resistance. Outside the cortex, coat layers of mainly proteins protect the endospore against damaging chemicals and enzymes (1). The StoA protein (also known as SpoIVH and YkvV) of *Bacillus subtilis* is a predicted membrane-bound thiol-disulfide oxidoreductase (TDOR)[4] important for endospore cortex synthesis (2, 3). Inactivation of the *stoA* gene results in spores deficient in the cortex layer that are much more sensitive than wild-type spores to heat, lysozyme, and chloroform treatment.

TDORs are proteins that catalyze the reduction of disulfide bonds and the oxidation of thiols. One pair of cysteine residues, often found in a -C*XX*C- motif, is present in the active site of TDORs, and although TDORs generally lack high overall sequence similarity, many of them share a common three-dimensional fold called the thioredoxin fold (4). Within the cell under normal circumstances, TDORs preferentially exhibit either a reducing or an oxidizing function as determined, at least in part, by the reduction potential of their disulfide/thiol active site. Their function is essential for the stabilization, folding, and activity of many proteins in bacterial cells, and they are involved in a wide range of processes, including cytochrome synthesis, cell motility, natural competence development, and toxin biosynthesis (5–8). Known enzymes that function in bacterial cell wall peptidoglycan synthesis, *e.g.* transglycosidases and transpeptidases, do not depend on cysteine redox chemistry, and so an important role for StoA in cortex synthesis was unexpected. Studies of this protein can reveal hitherto unknown features of sporulation and peptidoglycan synthesis (9). From the primary sequence of StoA (see Fig. 1), it was predicted to have one transmembrane segment and a single membrane-extruded domain with a thioredoxin-like fold. It is therefore likely to function in the control of thiol disulfide chemistry of a substrate protein(s). In the absence of BdbD, which is an orthologue of *Escherichia coli* DsbA that catalyzes disulfide

* This work was supported by a Federation of European Microbiological Societies research fellowship (to M. C. M.), by Swedish Research Council Grant 621-2007-6094, and by Wellcome Trust Grant 076017/Z/04/Z. The costs of publication of this article were defrayed in part by the payment of page charges. This article must therefore be hereby marked "*advertisement*" in accordance with 18 U.S.C. Section 1734 solely to indicate this fact.

⌘ *Author's Choice*—Final version full access.

The atomic coordinates and structure factors (code 3ERW) have been deposited in the Protein Data Bank, Research Collaboratory for Structural Bioinformatics, Rutgers University, New Brunswick, NJ (http://www.rcsb.org/).

[S] The on-line version of this article (available at http://www.jbc.org) contains supplemental Equations S1–S4, Table S1, and Figs. S1 and S2.

[1] Both authors contributed equally to this work.

[2] To whom correspondence may be addressed. Fax: 44-1603-592003; E-mail: n.le-brun@uea.ac.uk.

[3] To whom correspondence may be addressed. Fax: 46-46 2224113; E-mail: Lars.Hederstedt@cob.lu.se.

[4] The abbreviations used are: TDOR, thiol-disulfide oxidoreductase; Ches, *N*-cyclohexyl-2-aminoethanesulfonic acid; DTT, dithiothreitol; PEG, polyethylene glycol; MAL-PEG, monomethyl polyethylene glycol 5000 2-maleimidoethyl ether; Mops, 3-morpholinopropanesulfonate; TCEP, tris(2-carboxyethyl)phosphine hydrochloride; sStoA, soluble domain of *B. subtilis* StoA; GST, glutathione *S*-transferase; MALDI, matrix-assisted laser desorption ionization; TOF, time-of-flight; SAD, single wavelength anomalous dispersion.

TABLE 1
Strains and plasmids used in this work

Strain or plasmid	Genotype and/or relevant properties[a]	Origin or Ref.
E. coli		
BL21	F⁻ *ompT hsdS$_B$(r_B^- m_B^-) gal dcm*	Novagen
B834(DE3)	F⁻ *ompT hsdS$_B$(r_B^- m_B^-) gal dcm met* (DE3)	Novagen
MM294	*thi, pro, hsdR supE4*	45
TOP10	F⁻ *mcrA* Δ[*mrr-hsdRMS-mcrBC*] *F80lacZΔM15 ΔlacX74 recA1 araD139* Δ[*ara-leu*]*7697 galU galK rpsL endA1 nupG*	Invitrogen
B. subtilis		
1A1	*trpC2*	*Bacillus* Genetic Stock Center, Columbus, OH
LUL20	*trpC2 stoAΩpLLE39*; Cm^R	2
LUL30	*trpC2* Δ(*ykvU-stoA*)::*tet*; Tc^R	2
Plasmids		
pBluescript SK(+)	Cloning vector; Ap^R	Stratagene
pCR-Blunt-II-TOPO	Cloning vector; Km^R	Invitrogen
pDG148	Expression vector; Em^R Km^R	46
pGEX4T1	GST fusion expression vector; Ap^R	GE Healthcare
pLLE83	pDG148 derivative containing the *stoA* gene; Km^R	2
pLMC19	pBAD*myc*-HisC derivative encoding sStoA; Ap^R	This work
pLYM001	pBluescript SK(+) derivative containing *stoA* on a 2-kb fragment; Ap^R	This work
pLYM004	pLYM001 derivative encoding C68A StoA; Ap^R	This work
pLYM006	pLYM001 derivative encoding E71Q StoA; Ap^R	This work
pLYM009	pLYM001 derivative encoding C65A StoA; Ap^R	This work
pLYM012	pLLE83 variant encoding E71Q StoA; Km^R	This work
pLYM013	pLLE83 variant encoding C68A StoA; Km^R	This work
pLYM015	pLLE83 variant encoding C65A StoA; Km^R	This work
pLYM025	pCR-Blunt-II-TOPO containing *stoA*; Km^R	This work
pLYM028	pGEX4T1 derivative encoding GST-sStoA fusion protein; Ap^R	This work
pLYM031	pLYM028 variant encoding GST-sStoA with C65A mutation; Ap^R	This work
pLYM032	pLYM028 variant encoding GST-sStoA with C68A mutation; Ap^R	This work
pLYM033	pLYM028 variant encoding GST-sStoA with E71Q mutation; Ap^R	This work

[a] Ap^R, Cm^R, Em^R, Km^R, and Tc^R indicate resistance to ampicillin, chloramphenicol, erythromycin, kanamycin, and tetracycline, respectively.

bond formation in proteins on the outside of the cytoplasmic membrane, StoA is no longer important for endospore cortex synthesis, indicating that it functions to specifically reduce disulfide bonds on the outside of the cytoplasmic membrane (2). It was also proposed that the protein most likely operates in the intermembrane space of the developing forespore where the cortex is synthesized. The substrate protein(s) of StoA with a function in cortex synthesis has not yet been identified, but the CcdA protein most likely functions in transmembrane transport of reducing equivalents from thioredoxin in the cytoplasm to StoA in the forespore intermembrane space (9, 10).

StoA is similar in primary sequence to ResA (see Fig. 1), which is a ditopic membrane-bound TDOR that functions specifically as a reductase in cytochrome *c* maturation in *B. subtilis* and which has been well characterized (11). The soluble, membrane-extruded part of ResA has a typical thioredoxin fold augmented by an additional β-hairpin at the N-terminal end and a σ/β insertion between strand β2 and helix α2 of the classic thioredoxin fold (12). The cysteine residues of the ResA active site exhibit unusually high pK_a values (both above 8) (13), yielding very low reactivity of the cysteine residues at neutral pH. In contrast to most other TDORs that have been characterized, both thiols of the ResA active site are reactive to thiol-modifying reagents. In addition, a glutamate (Glu-80) in the vicinity of the active site has been shown to play a key role in controlling the reactivity of the enzyme (13, 14). StoA is not involved in cytochrome *c* synthesis and cannot functionally replace ResA. Likewise ResA cannot replace StoA in sporulation (2). Thus, StoA and ResA have distinctly different substrate specificities. Given their primary sequence similarity, it is of key importance to understand the basis of their specificity differences.

Here we report the isolation of the soluble domain of *B. subtilis* StoA (sStoA) and subsequent three-dimensional structure determination together with the biophysical characterization of the protein, including reduction potential and pK_a values of the active site cysteines. Furthermore mutant variants of StoA with amino acid substitutions in the active site region have been studied *in vitro* and *in vivo* in *B. subtilis*. Common and discriminating features of StoA and ResA are discussed in the context of the distinctly different substrate specificities exhibited by these similar proteins.

EXPERIMENTAL PROCEDURES

Bacterial Strains and Growth of Bacteria—Strains used in this work are presented in Table 1. *E. coli* strains were grown in lysogeny broth or on lysogeny broth plates, and *B. subtilis* strains were grown in nutrient sporulation medium with phosphate (15) with appropriate antibiotics added as follows: ampicillin, 100 μg/ml; kanamycin, 10 μg/ml (for *B. subtilis*) or 50 μg/ml (for *E. coli*); and chloramphenicol, 3 or 4 μg/ml (for *B. subtilis*) and 15 μg/ml (for *E. coli*). Liquid cultures were grown in baffled E-flasks on a rotary shaker (200 rpm) at 37 °C.

Construction of Plasmids Encoding sStoA—For production of sStoA plasmid pLMC19 was constructed by amplifying part of the *stoA* gene using oligonucleotides LE051 and LE052 (supplemental Table S1), Phusion polymerase (Finnzymes), and *B. subtilis* 1A1 chromosomal DNA as template. The PCR product was cloned into pCR®-Blunt-II-TOPO® (Invitrogen). The insert was cut out from the plasmid using PstI and HindIII and ligated into pBADmyc-HisC cut with the same enzymes resulting in plasmid pLMC19. The cloned *stoA* fragment was verified by DNA sequence analysis.

For production of a thrombin-cleavable GST-sStoA fusion protein, a fragment of the *stoA* gene encoding residues 21–165 of StoA was first amplified by PCR as above using oligonucleo-

tides LY001 and LY002 as primers and subsequently cloned into pCR-Blunt-II-TOPO generating pLYM025, which was verified by sequencing. pLYM025, propagated in *E. coli* strain MM294, was digested by BamHI and SalI, and the *stoA* fragment was cloned into pGEX4T1, resulting in pLYM028.

For the construction of plasmids encoding mutant StoA variants, pLLE83 was digested by HindIII and BamHI, and the 2-kb fragment containing *stoA* was cloned in pBluescript SK(+), resulting in pLYM001. Site-directed mutagenesis was carried out with the QuikChange II kit and protocol (Stratagene) using pLYM001 and primers LY003–LY008 to generate plasmids pLYM009 (C65A), pLYM004 (C68A), and pLYM006 (E71Q), respectively, which were verified by sequencing. The HindIII/BamHI fragment of each of these three plasmids was subsequently cloned into pDG148, generating, respectively, pLYM015, pLYM013, and pLYM012, which were used for expression of full-length mutant *stoA* genes in *B. subtilis*. Plasmids encoding GST-sStoA fusion protein with C65A or C68A in sStoA were obtained by first amplifying *stoA* as above using primers LY001 and LY002 and pLYM009 or pLYM004 plasmid DNA, respectively, as template. PCR products were then cloned into pGEX4T1 as described above for the wild-type variant, generating plasmids pLYM031 and pLYM032, which were verified by sequencing.

Purification of sStoA—Non-tagged sStoA, which was utilized in initial crystallization trials and to generate a StoA antiserum, was purified from *E. coli* TOP10/pLMC19 as described in the supplemental data. For the production of GST-sStoA fusion protein, *E. coli* BL21/pLYM028 was grown in 1-liter portions in 5-liter E-flasks. At A_{600} = 0.6–0.8 expression was induced by addition of 1 mM isopropyl β-D-thiogalactoside (final concentration). After incubation for 5 h, cells were collected by centrifugation, washed in PBS (140 mM NaCl, 2.7 mM KCl, 10 mM Na_2HPO_4, 1.8 mM KH_2PO_4, pH 7.3), and stored as pellets at −20 °C until required. The cell pellet from 1 liter of culture was suspended in 20 ml of ice-cold PBS containing 1 mM DTT and lysed by passage (three times) through a French pressure cell at 18,000 p.s.i. The lysate was centrifuged at 48,000 × *g* for 40 min at 4 °C, and the supernatant was centrifuged at 100,000 × *g* for 1 h at 4 °C. The final supernatant was mixed with 2 ml of 50% slurry of glutathione-Sepharose 4B (GE Healthcare), and the GST-sStoA fusion protein was purified according to the resin manufacturer's instructions. Affinity-purified GST-sStoA fusion protein was cleaved by 50 units of thrombin (GE Healthcare) at room temperature for 5 h and then loaded onto a Sephacryl S-100 HR gel filtration column. Protein was eluted using 20 mM Tris-HCl, pH 8.0, containing 100 mM NaCl and 1 mM DTT. Fractions containing sStoA were identified using SDS-PAGE and Western blot with StoA antiserum, pooled, and concentrated. The N-terminal amino acid residue sequence of the purified protein was verified by Edman degradation (see Fig. 1). Cysteine variants of sStoA were produced in *E. coli* BL21 containing pLYM031 or pLYM032 and purified as described for wild-type sStoA.

For the production of selenomethionine-labeled sStoA, *E. coli* B834(DE3)/pLYM028 was grown overnight in 10 ml of SelenoMet™ medium (AthenaES) supplemented with 50 μg/ml methionine. The overnight culture was used to inoculate 1 liter of SelenoMet medium containing 50 μg/μl methionine to an A_{600} of 0.1, and the culture was grown until A_{600} was ~0.8. Cells were harvested by centrifugation for 10 min at 10,000 × *g* at 4 °C, and the pellet was resuspended in 1 liter of non-supplemented SelenoMet medium and incubated for 2 h. Selenomethionine was then added to a final concentration of 50 μg/ml, and the culture was incubated for a further 30 min when production of GST-sStoA was induced by the addition of 1 mM isopropyl β-D-thiogalactoside (final concentration). Four hours after induction the culture was harvested by centrifugation for 10 min at 10,000 × *g* at 4 °C. The cells were washed in cold PBS and stored as a pellet at −20 °C. Selenomethionine-labeled sStoA was purified as described above. MALDI mass spectrometry confirmed that selenomethionine incorporation was close to 100%.

Crystallization and Structure Determination of sStoA—sStoA was crystallized using the sitting drop vapor diffusion method. A 2-μl sitting drop was formed by mixing equal volumes of protein solution (12 mg/ml sStoA in 25 mM Mops, pH 7.0) and crystallization reagent (27% (w/v) PEG 2000, 0.2 M ammonium acetate, 100 mM sodium acetate, pH 4.8) over an 800-μl reservoir of the reagent alone. Crystals grew over a period of 1–2 days and were cryoprotected in a solution of 30% (w/v) PEG 2000, 100 mM sodium acetate, pH 4.8, 20% (v/v) ethylene glycol before flash freezing in liquid nitrogen. X-ray data sets for native and selenomethionine-labeled sStoA were collected on beam line ID23-1 of the European Synchrotron Radiation Facility (Grenoble, France). Structure determination utilized programs of the CCP4 (16) and PHENIX (17) software suites. Diffraction patterns were indexed and integrated with MOSFLM (18) and scaled with SCALA (19). Selenium sites were identified using a combination of automated methods implemented in PHENIX.HYSS and manual inspection of anomalous difference maps produced with FFT. An initial electron density map was obtained using SAD phases calculated with MLPHARE and subsequent density modification with DM. A key factor in producing an interpretable electron density map was the identification of the correct non-crystallographic symmetry relating each sStoA molecule in the asymmetric unit. Non-crystallographic symmetry averaging in the phase improvement procedure benefited from the use of a predefined protein mask derived from a monomer of ResA (12). Further phase improvement was obtained by cross-crystal averaging with a second SAD-phased selenomethionine data set composed of merged data from two individual sStoA crystals. Manual model building was conducted in COOT, and initial phased refinement of the model was conducted with REFMAC (20). Further refinement of the model (against a single selenomethionine data set with a "low" twin fraction (α = 0.36)) utilized PHENIX.REFINE, which was essential for proper refinement of the twinned data. The final model of sStoA is composed of seven ordered protein chains and 99 water molecules. A small amount of residual density located at a coordinate of (42.34, 64.52, 19.53) may indicate the presence of an additional StoA monomer of low occupancy and high mobility that is insufficiently well resolved to enable further model building. The

coordinates and structure factors have been deposited at the Protein Data Bank with accession code 3ERW.

Reduction Potential Determination—sStoA (0.2 μM) in 50 mM potassium phosphate, pH 7, was added to 5 mM oxidized DTT in the same buffer to obtain the fully oxidized protein. The protein was subsequently titrated with reduced DTT in the same buffer, allowing 10 min for the protein to equilibrate to each new potential. The transition from oxidized to reduced protein was monitored by the increase in tryptophan fluorescence emission at 344 nm (excitation at 280 nm) measured at 25 °C using a PerkinElmer Life Sciences LS-55 fluorescence spectrometer with 10-nm excitation and emission slits. Intensity was corrected for dilution effects. From the data at 344 nm, midpoint reduction potentials were determined as described previously (11, 21); further details are given in the supplemental data.

pH Stability and Cysteine pK_a Measurements—Reduced wild-type and variant sStoA protein stocks were prepared in 10 mM Mops, pH 7, 2 mM TCEP (Pierce) and subsequently diluted (30-fold to a final protein concentration of 0.15 μM) with PCTC (potassium phosphate, sodium citrate, Tris, and Ches, all at 50 mM) buffer (pre-prepared at the appropriate pH) and equilibrated in a sealed cuvette for 1 h before measurement of tryptophan fluorescence spectra as above. For pK_a measurements, reduced protein solutions (wild-type sStoA and single cysteine variants) were prepared in 10 mM Mops, pH 7, with 2 mM TCEP as reductant. Reaction with 6-bromoacetyl-2-dimethylaminonaphthalene was carried out under pseudo-first order conditions, and pK_a values were determined as described previously (13). Further details are also given in the supplemental data.

Modification of sStoA with MAL-PEG—Wild-type sStoA and C65A and C68A variant proteins in 20 mM Tris-HCl, 100 mM NaCl, pH 8.0 were treated with 1 mM TCEP at room temperature for 30 min. Excess TCEP was removed using a YM10 column (Millipore), and each reduced sStoA sample (10 μg) was incubated with 0.1 mM or 1 mM monomethyl polyethylene glycol 5000 2-maleimidoethyl ether (MAL-PEG) (≥90%; Fluka) at room temperature for 30 min. The samples were then applied directly onto an SDS-polyacrylamide gel.

Antisera and Western Blot Analysis—Non-tagged sStoA was used to immunize rabbits (custom polyclonal antibody production service; MedProbe, Oslo, Norway). For Western blot analysis, proteins were separated by SDS-PAGE using the Schägger and von Jagow (22) system and subsequently electroblotted to a polyvinylidene difluoride membrane (Millipore) by wet blot using 20 mM Tris, 150 mM glycine, 20% (v/v) methanol. Transfer conditions were 30 V, 0.1 A overnight at 4 °C. The membrane was blocked using 5% (w/v) nonfat dry milk in 0.1% (v/v) Tween 20 in PBS. StoA antiserum was used at 1500-fold dilution. Bound primary antibodies were detected using horseradish peroxidase-linked anti-rabbit antiserum from donkey (GE Healthcare) diluted 3000-fold. Immunodetection was carried out by chemiluminescence using SuperSignal West Pico substrate (Pierce) and an Eastman Kodak Co. image station.

Preparation of Cell-free Extracts from B. subtilis Strains—Samples of 200 ml were taken from a 1.5-liter culture at time points spanning from 1 h before entry into postexponential ($T = -1$) to 5 h into stationary growth phase ($T = 5$). Cells were harvested by centrifugation; immediately washed in 50 mM potassium phosphate, pH 8.0; and frozen as a pellet at −20 °C. When required, cell pellets were thawed and suspended in 0.8 ml of phosphate buffer containing 0.7 mg/ml lysozyme, 25 μg/ml DNase, 25 μg/ml RNase, 4 mM $MgSO_4$, and Complete protease inhibitor (Roche Applied Science; one tablet/50 ml of buffer)). After incubation at 37 °C for 45 min, an aliquot was frozen for subsequent analysis of total cell lysate. The remaining main part of the lysate was centrifuged at 48,000 × *g* for 60 min at 4 °C: the supernatant was used for the analysis of the soluble cell fraction, whereas the pellet, after washing in phosphate buffer, was suspended in 0.3 ml of the buffer and used for the analysis of the membrane fraction.

Other Methods—Chromosomal DNA from *B. subtilis* was isolated according to Marmur (23). *E. coli* was transformed by electroporation (24). Plasmid DNA was isolated using Quantum miniprep (Bio-Rad) or by CsCl density gradient centrifugation. SDS-PAGE was carried out using the NuPAGE system (Invitrogen) or Schägger and von Jagow (22) system. Protein concentrations were determined by measuring the absorbance at 280 nm using an extinction coefficient of 15,460 ± 100 M^{-1} cm^{-1} determined as described previously (25) or using the BCA reagent (Bio-Rad) with bovine albumin as reference.

N-terminal sequencing was carried out by Edman degradation (Protein Analysis Center, Karolinska Institutet, Sweden) on proteins separated by SDS-PAGE and electroblotted onto a polyvinylidene difluoride membrane as described for Western blotting. The membrane was stained with 0.1% (w/v) Coomassie Brilliant Blue R-250 in 2% (v/v) acetic acid, 45% (v/v) methanol. Mass spectrometry analysis was performed using an UltraFlex-MALDI-TOF/TOF mass spectrometer (Bruker Daltonics, Coventry, UK) on samples prepared by mixing sStoA in a 1:1 ratio with a saturated solution of sinapinic acid matrix in 30% acetonitrile, 0.05% trifluoroacetic acid. 0.5 μl of this combined mixture was spotted onto a polished stainless steel target and allowed to crystallize prior to analysis. The spectrometer was externally calibrated using a two-point linear calibration through the singly and doubly charged ions of trypsinogen.

The molecular mass of sStoA was determined using high performance liquid chromatography with an Ultraspherogel SEC 3000 column (Beckman). 1.2 nmol of sStoA in 10 μl was applied to the column equilibrated with 20 mM Tris-HCl, pH 8.0, 0.15 M NaCl, 1 mM DTT and eluted in the same buffer at a flow rate of 1 ml min^{-1}. Mass was calculated based on a calibration curve obtained using catalase (230 kDa), bovine serum albumin (67 kDa), ovalbumin (46 kDa), carboanhydrase (26 kDa), myoglobin (17.2 kDa), and horse heart cytochrome *c* (12.3 kDa).

RESULTS AND DISCUSSION

StoA Is a Membrane-bound Protein—From its amino acid sequence (Fig. 1), StoA was predicted to be a ditopic membrane-bound protein with an N-terminal ~30-residue segment that anchors the ~135-residue TDOR domain to the membrane. As shown previously by the use of a StoA-PhoA (alkaline phosphatase) fusion protein in *E. coli* cells, the transmembrane segment of StoA functions as a signal sequence to direct translocation and to membrane anchor the C-terminal TDOR

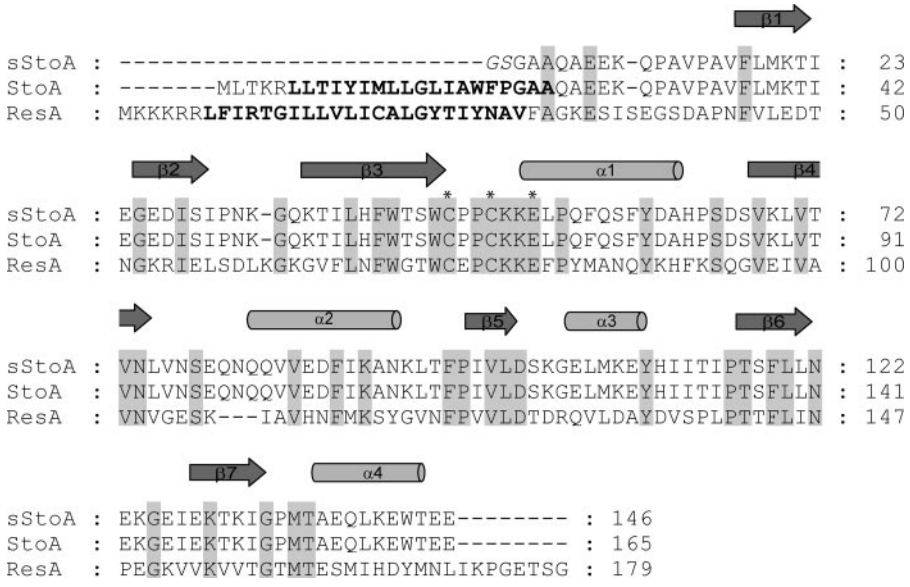

FIGURE 1. **Amino acid residue sequence alignment of *B. subtilis* sStoA used in structural and biochemical analyses, full-length StoA, and full-length ResA proteins.** Invariant residues are marked in *gray*. The N-terminal sequence of sStoA is as confirmed by Edman degradation. Vector pGEX4T1-encoded residues in sStoA are indicated in *italics*. The predicted transmembrane segments of StoA and ResA are in *bold letters*. *Stars* indicate the active site residues Cys-65 and Cys-68 and conserved residue Glu-71 of StoA. Secondary structural elements are indicated *above* the sequence. The alignment was obtained using AlignX, Vector NTI Suite 6.0.

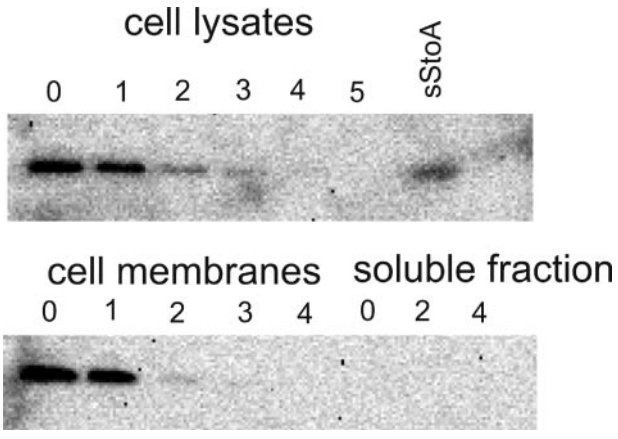

FIGURE 2. **Subcellular localization of StoA.** Western blot analysis of total cell-free lysates, membrane fractions, and soluble fractions of *B. subtilis* 1A1/pLLE83 for StoA antigen is shown. Cells were harvested at different time points during growth in nutrient sporulation medium with phosphate. Time point 0 is at the entry of stationary growth phase, and subsequent *numbers* indicate hours into stationary phase. *sStoA* indicates a sample of purified sStoA loaded on the gel as a reference. Approximately 20 μg of cell protein was loaded in each lane except for purified sStoA where 20 ng was loaded.

domain (2). Experiments in *B. subtilis* indicated that the function of StoA is not dependent on the membrane anchor (3), and prediction programs suggested that the N-terminal segment might be cleaved off after the TDOR domain has been translocated across the membrane. To establish whether StoA is a membrane-bound protein, *B. subtilis* strain 1A1 was grown in nutrient sporulation medium with phosphate for sporulation, and samples taken at different time points during growth were analyzed for StoA by using Western blot with polyclonal antiserum directed against the TDOR domain of StoA. No StoA antigen could be detected in cell-free extracts, although BdbD, a protein very similar to StoA, was readily detected in all samples (not shown). To facilitate detection of StoA by increasing the level of the protein in cells, plasmid pLLE83 containing *stoA* under control of the pSpac promoter was used. StoA was found in the membrane fraction of 1A1/pLLE83 cells from early stationary phase cultures but not in late stationary phase cultures (Fig. 2). The results indicate that StoA is membrane-associated but is present in very low amounts and is degraded or trapped in maturing endospores so that it is not detectable by the Western blot procedure used.

In Vivo Functional Analysis of Active Site Variants of StoA—To establish that the function of StoA in endospore biogenesis is dependent on the cysteine residues of the protein, *B. subtilis* strain LUL20 in which the *stoA* gene is inactivated and strain LUL30 in which *stoA* is deleted from the chromosome were used (2). These two strains containing a plasmid encoding wild-type StoA (pLLE83), C65A StoA (pLYM015), C68A StoA (pLYM013), or empty vector (pDG148) were grown for sporulation and tested for production of heat-resistant cells. Western blot analysis showed that StoA proteins were present in membranes of strains containing pLYM015 and pLYM013 (see supplemental Fig. S1). Compared with wild type, the presence of either StoA variant resulted in a ~100-fold reduction in sporulation efficiency (Table 2). Cells completely lacking StoA, however, showed more than a 1000-fold reduction in sporulation efficiency indicating some residual activity of StoA even when one of the two cysteine residues is missing.

The High Resolution Structure of the Soluble Domain of StoA in a Mixture of Oxidized and Reduced States—sStoA (residues 22–165) was produced in *E. coli* and purified. Gel filtration analysis indicated a molecular mass of 17 ± 3 kDa (data not shown) consistent with the protein being monomeric in solution. The crystal structure of sStoA was solved using the selenomethionine SAD method of phase determination. The crystals used in structure determination belong to space group $P3_1$ and contained seven molecules of sStoA per asymmetric unit (see supplemental Fig. S2). Although structure determination was hampered by the fact that sStoA crystals were merohedrally twinned, it was nonetheless possible to refine the structure to acceptable R_{work} and R_{free} values using twin refinement against x-ray data obtained from a single sStoA crystal with a twin fraction (α) of 0.36. Data collection and refinement statistics for the sStoA structure are given in Table 3.

Overall the structure of each sStoA monomer (Fig. 3*A*) can be described as a modified thioredoxin-like fold that is highly reminiscent of *B. subtilis* ResA (12), CcmG (from *E. coli* and *Bradyrhizobium japonicum*) (26, 27), and *Mycobacterium tuberculosis* DsbE (28), which are all extracytoplasmic TDORs (see Fig. 3*B*). Like these proteins, the classical thioredoxin-like motif of StoA is embellished by a central

TABLE 2

Efficiency of *B. subtilis* strains in producing heat-resistant cells after growth for 2 days at 37 °C in nutrient sporulation medium with phosphate supplemented with 1 mM isopropyl β-D-thiogalactoside

Presented are typical results obtained from at least two independent experiments with each strain, including analysis of two sister clones. *B. subtilis* LUL20 and LUL30 are StoA-deficient, and 1A1 is the parental strain (Table 1).

Strain	StoA variant encoded by plasmid	Viable count before heating	Viable count after 15 min at 80 °C	Sporulation efficiency[a]
				%
1A1		4.0×10^8	3.4×10^8	85
LUL20		5.5×10^7	2.0×10^4	<0.05
LUL20/pDG148		4.7×10^7	1.2×10^4	<0.05
LUL20/pLLE83	Wild type	2.6×10^8	1.3×10^8	50
LUL20/pLYM015	C65A	4.9×10^7	3.7×10^5	0.7
LUL20/pLYM013	C68A	7.4×10^7	5.0×10^5	0.7
LUL20/pLYM012	E71Q	4.1×10^7	2.1×10^6	5.1
LUL30		1.9×10^7	1.4×10^4	<0.05
LUL30/pDG148		2.1×10^7	3.7×10^4	<0.05
LUL30/pLLE83	Wild type	1.4×10^8	8.6×10^7	61
LUL30/pLYM015	C65A	4.9×10^7	9.2×10^4	0.2
LUL30/pLYM013	C68A	4.6×10^7	6.2×10^4	0.1
LUL30/pLYM012	E71Q	3.9×10^7	1.6×10^5	0.4

[a] Viable count after heat treatment divided by that before heating.

TABLE 3

X-ray data collection and refinement statistics for sStoA

Se-Met, selenomethionine; r.m.s., root mean square. Values in parentheses represent the highest resolution shell.

	Two-crystal merged Se-Met data set	Hires Se-Met data set
Space group	$P3_1$	$P3_1$
Cell parameters (Å)	$a = b = 133.74$, $c = 64.82$	$a = b = 133.72$, $c = 64.82$
Energy (eV)	12,656.6	12,656.6
f'	−7.79	−7.79
f''	6.38	6.38
Twinning operator	$-k, -h, -l$	$-k, -h, -l$
Twinning fraction	0.38	0.36
Resolution (Å)	43.19-2.60 (2.74-2.60)	36.27-2.50 (2.64-2.50)
R_{sym}	0.154 (0.565)	0.083 (0.293)
I/σ	18.9 (4.0)	16.1 (3.3)
Anomalous completeness (%)	99.4 (96.0)	97.2 (83.8)
Anomalous multiplicity	5.0 (3.6)	2.5 (1.7)
Unique observations		44,319 (6,023)
R		0.1787
R_{free}		0.2011
r.m.s. bond (Å)		0.040
r.m.s. angle (°)		2.191

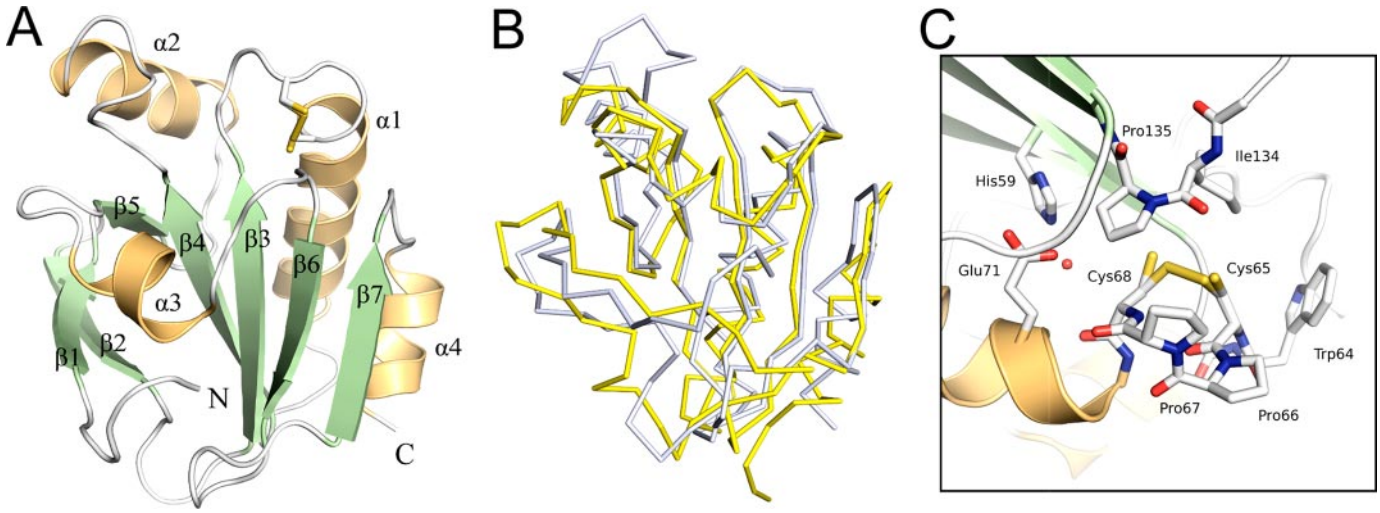

FIGURE 3. **The three-dimensional structure of the soluble domain of StoA.** *A*, three-dimensional structure of sStoA showing that the protein exhibits a classical thioredoxin-like fold with two significant insertions: the N-terminal region contains a two-stranded, antiparallel hairpin, whereas the central insert, located after the β3-α1-β4 motif of the thioredoxin fold, comprises one helix (α2) and one strand (β5). Secondary structure elements are labeled from the N terminus (with the N-terminal transmembrane helix being 0), and the N and C termini of sStoA are indicated. *B*, overlay of the StoA (*gray*) and reduced ResA (*yellow*) peptide backbones (in ribbon representation). *C*, the active site region of StoA showing the CPPC motif, surrounding residues, and a buried water molecule (*red sphere*). All structural figures were prepared with PyMOL (44) and annotated with GIMP.

αβ insertion and an N-terminal β-hairpin (in addition to the transmembrane helix predicted from primary sequence analysis). Unlike other extracytoplasmic TDORs, StoA also possesses a short insertion of residues between strand β4 and helix α2 that forms an ordered loop at the surface of the protein.

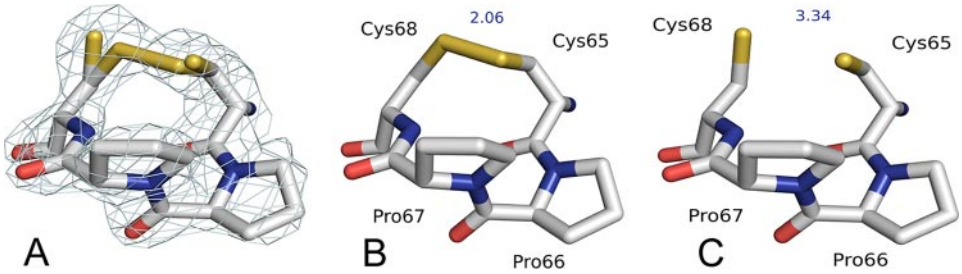

FIGURE 4. **The active site of StoA in oxidized and reduced states.** *A*, electron density (contoured at 1.2 σ) of the active site CPPC motif of StoA reveals a mixture of oxidized and reduced states. *B* and *C*, separated representations of the active site region in oxidized and reduced states, respectively. Intercysteine sulfur distances are indicated (in Å).

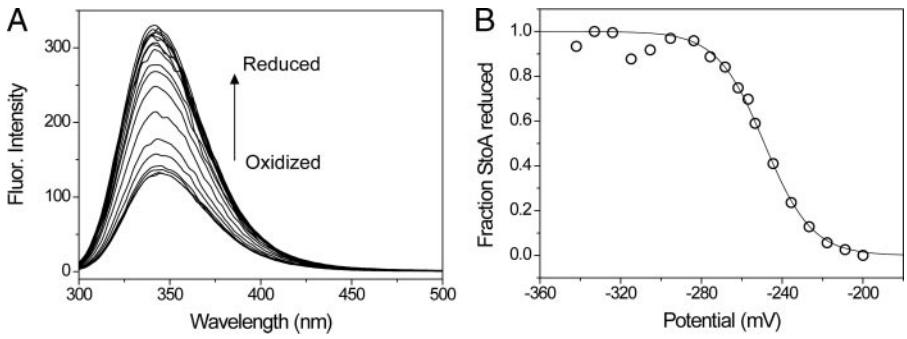

FIGURE 5. **Redox titration of sStoA.** *A*, fluorescence spectra of sStoA in 50 mM potassium phosphate, 5 mM oxidized DTT, pH 7.0 following incubation with increasing concentrations of reduced DTT at 25 °C. *B*, plot of fraction of reduced sStoA (calculated from the fluorescence (*Fluor.*) intensity at 344 nm as described in the supplemental data) as a function of the cell potential. The *solid line* shows a fit to supplemental Equation S1.

In the structure determined here, the active site cysteines of sStoA appear as a mixture of oxidized and reduced redox states (in each monomer). Crystallization of sStoA utilized solely the oxidized form of the protein, and thus it is likely that partial reduction of the disulfide bond was induced by photoreduction in the x-ray beam. The electron density associated with the partially broken disulfide is shown in Fig. 4*A* along with separated models of the oxidized and reduced conformations shown in Fig. 4, *B* and *C*, respectively.

The oxidized (disulfide-bonded) conformation of the active site dominates the electron density and is best described as adopting a classical right-handed hook conformation with a $\chi 3$ angle of 73.5 ± 1.8° formed between the two cysteine residues. The sulfur-to-sulfur bond distance for the oxidized conformation is 2.06 Å, whereas in the reduced conformation an average sulfur-to-sulfur distance of 3.4 Å separates the cysteine residues. This distance is considerably shorter than that observed for the structure of ResA that has an exceptionally long sulfur-to-sulfur distance of 4.5 Å in the reduced state (12). Partial reduction of the disulfide does not seem to cause significant rearrangement of the local protein structure, and thus, unlike ResA, there is no evidence for any redox-linked conformational changes due to reduction of the cysteines in StoA.

In almost all known natural thioredoxin-like proteins, at least one of the two residues that intervene between the active site cysteines residues (*i.e.* within the C*XX*C motif) is a proline. In StoA, *both* of these intervening residues are proline. Pro-66 and Pro-67 both adopt the *trans* conformations and have backbone ϕ-ψ angles that are consistent with an α-helical conformation. Like all other thioredoxin-like TDORs, the C*XX*C motif of StoA is found at the N terminus of a reasonably long α-helix ($\alpha 1$ in StoA), and the macrodipole arising from this helix is often invoked as a primary cause of the lowered pK_a values associated with the more N-terminal cysteine residue of the C*XX*C motif in most TDORs (29). The presence of proline residues at the cap of this active site helix in StoA is therefore likely to have important consequences for the distribution of the electrostatic field near the cysteines as proline does not possess a standard peptide group. Furthermore the limited conformational freedom of proline (in comparison with other residues) may be an important factor in maintaining rigidity of the CPPC motif and may be one of the reasons that the reduced form of sStoA is so similar to its oxidized form.

A further proline residue (Pro-135), which is in the *cis* conformation and is conserved in all thioredoxin-like proteins, is found in van der Waals contact with two buried polar residues, a histidine and a glutamate, which are located immediately behind the second cysteine of the active site motif. His-59 is located on strand $\beta 3$, whereas Glu-71 arises from helix $\alpha 1$ directly opposite. A buried water molecule is observed in the space between these two residues within hydrogen-bonding distance of the Cys-68 sulfur (see Fig. 3*C*).

The arrangement of these two buried polar residues and the intervening water molecule (in StoA) is very similar to that observed in ResA where the glutamate is conserved (Glu-80) and an asparagine (Asn-68) residue takes an equivalent position to that of His-59. Substitution of Glu-80 in ResA has been shown previously to have a significant effect on the active site properties of the enzyme; for example, the pK_a values of both active site cysteines were significantly lowered in an E80Q variant (13), and a *B. subtilis* strain containing E80Q ResA was also severely impaired in its ability to mature *c*-type cytochromes (14). Thus, it may be that these buried polar residues are also important in StoA function. To analyze the functional role of residue Glu-71 in StoA, the StoA-deficient *B. subtilis* strains LUL20 and LUL30 containing plasmid pLYM012 encoding E71Q StoA were studied. The presence of the variant StoA protein in membranes was confirmed by Western blot (supplemental Fig. S1), and the efficiency in production of heat-resistant endospores was found to be 10–150-fold (depending on strain) lower in these strains compared with wild-type controls (Table 2). This indicates that Glu-71 is functionally important in StoA.

StoA Is a Low Potential TDOR—The reduction potential of the active site cysteines of sStoA was measured using the difference in tryptophan fluorescence intensity of oxidized and reduced sStoA to follow oxidation state as a function of reduc-

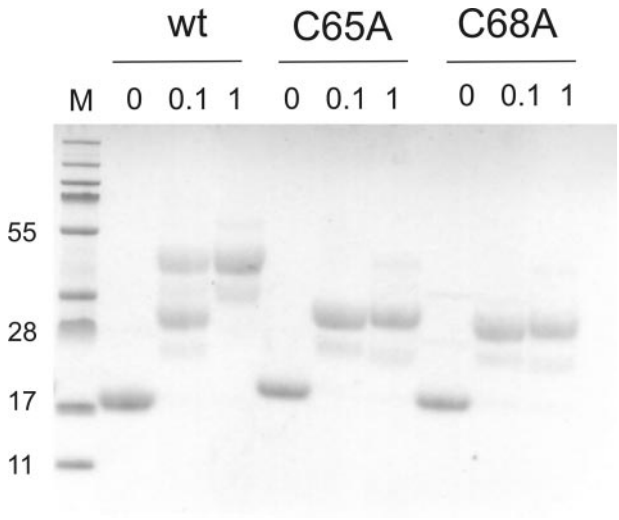

FIGURE 6. **Reactivity of the active site cysteines of sStoA.** SDS-PAGE of purified reduced wild-type (*wt*) sStoA and C65A and C68A sStoA following reaction with MAL-PEG is shown. The protein variants were incubated with 0, 0.1, and 1 mM MAL-PEG before electrophoresis as indicated, and the gel was stained for protein. The lane indicated *M* contains molecular mass (kDa) markers.

tion potential (see Fig. 5). The data fitted well to the Nernst equation, giving a midpoint reduction potential of −248 ± 2 mV *versus* normal hydrogen electrode at pH 7 with $n = 2.18 \pm 0.16$, as expected for a two-electron reduction process. This value is similar to that measured for *B. subtilis* ResA (−256 mV at pH 7) (21) and *E. coli* thioredoxin (−270 mV at pH 7) (30, 31) and is entirely consistent with the structural similarity between these proteins and a role for StoA in the reduction of (as yet unidentified) proteins involved in endospore cortex synthesis (2, 9).

Both Active Site Cysteines Can Be Modified by Alkylating Agents—The solvent accessibility of the active site cysteines of wild-type sStoA and two variants, C65A and C68A sStoA, was investigated using MAL-PEG, a high molecular mass, cysteine-specific alkylating agent. sStoA proteins were incubated with either 0, 0.1, or 1 mM MAL-PEG as described under "Experimental Procedures" and analyzed by SDS-PAGE. Samples with exposed thiols are able to react with the MAL-PEG to form covalent complexes of significantly greater molecular mass relative to non-alkylated samples and thus are retarded during subsequent migration in the electrophoretic gel (see Fig. 6). Unmodified wild-type, C65A, and C68A sStoA variants migrated with an apparent molecular mass of ~18 kDa, which is in reasonable agreement with the actual mass (16.4 kDa). In the presence of MAL-PEG, both single cysteine variants reacted to give a single species with a significantly lower mobility. Protein molecular mass standards cannot be used to judge the mass of MAL-PEG-modified proteins, but the significant retardation of sStoA variants is consistent with the alkylation of a single cysteine residue in each. In contrast, wild-type sStoA gave rise to two bands when incubated with 0.1 mM Mal-PEG. The lower (faster running) band corresponded to the singly modified single cysteine variants, and we conclude that under these conditions sStoA is present as a mixture of singly and doubly modified molecules. This was confirmed by incubating sStoA with a higher (1 mM) concentration of MAL-PEG that resulted in the observation of only the larger, slower running band corresponding to the doubly modified protein. In addition to these major bands, other much fainter bands were observed on the gel; these most likely arise from a small degree of heterogeneity in the size of the PEG adducts in the MAL-PEG reagent and therefore do not represent additional (non-cysteine) alkylation events or protein heterogeneity. Certainly no protein heterogeneity was observed in any of the untreated sStoA samples.

From the structure it is apparent that the more N-terminal of the two active site cysteines is exposed to the solvent, whereas the other is not. Solvent-accessible surface area calculations (using a solvent probe of 1.2 Å) on the structure of reduced sStoA showed that the Cys-65 sulfur has an accessible surface area of 5.43 $Å^2$, whereas the sulfur atom of Cys-68 is inaccessible from the bulk solvent. A similar arrangement exists in all structurally characterized thioredoxin-like proteins, and in virtually all of them, the second, buried cysteine thiol does not react with modifying reagents in solution (32, 33). This is not the case for *B. subtilis* ResA in which we showed previously that both cysteines are readily modified by alkylating reagents (13). To our knowledge, ResA and now StoA are the only examples where this behavior has been demonstrated. For StoA, one possibility is that alkylation of the solvent-exposed Cys-65 might cause a structural rearrangement that allows subsequent modification of Cys-68. Alternatively the reduced protein in solution may undergo dynamic motion that would allow occasional access to the sulfur of Cys-68.

pK_a Values of StoA Active Site Cysteines—The pH stability profiles of the wild-type and single cysteine variant sStoA proteins were first determined to verify the range of values over which the acid-base properties of each protein could be investigated. The intrinsic tryptophan fluorescence was measured as a function of pH for each protein under reducing conditions. Significant changes in the character of the tryptophan fluorescence emission spectrum, resulting from unfolding of the proteins, were observed at extremes of pH. Both the emission wavelength maxima and fluorescence intensity maxima were affected by pH-induced unfolding. The former has the advantage of being independent of protein concentration and was thus used preferentially in monitoring pH stability (see Fig. 7). The data showed that wild-type sStoA is stable between pH 3.5 and 9.3, whereas C65A and C68A sStoA variants are stable between 4.4 and 9.6 and between 3.7 and 9.3, respectively.

The acid-base properties of the active site cysteines of wild-type sStoA and the C65A and C68A variants were investigated by measuring rates of reaction with the fluorescent probe 6-bromoacetyl-2-dimethylaminonaphthalene as described under "Experimental Procedures" (see Fig. 8*A*). The fluorescence is sensitive to the environment of the modified cysteine with emission occurring in the range of ~440–550 nm, depending on the solvent exposure of the modified cysteine (34). Here the emission maxima for Cys-65 and Cys-68 were 510 nm, indicating that the fluorescent group of both modified residues is located in a relatively solvent-exposed position. For the single cysteine variants of sStoA, data fitted well to an equation describing a single protonation/deprotonation event, giving pK_a values of 7.0 ± 0.1 and 7.1 ± 0.1 for Cys-65 and Cys-68, respectively (see Fig. 8, *C* and *D*). For the wild-type protein in

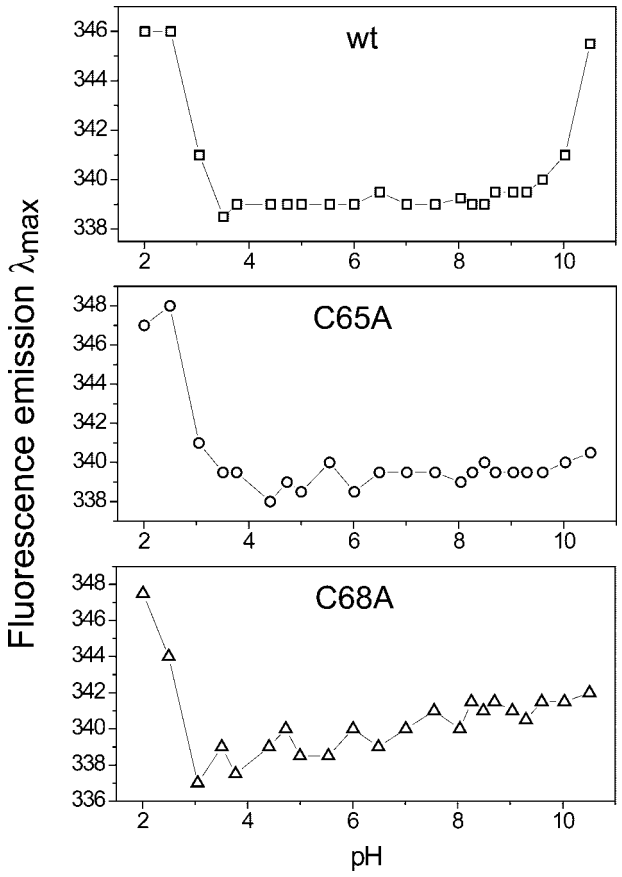

FIGURE 7. **pH stability of wild-type and variant sStoA proteins monitored by fluorescence.** Plots of tryptophan fluorescence emission maxima as a function of pH for solutions of wild-type (*wt*) sStoA and C65A and C68A sStoA as indicated (all at 0.15 μM in PCTC buffer) as a function of pH are shown.

which both cysteine residues are intact, the data fitted well to two independent protonation/deprotonation events, giving pK_a values of 5.5 ± 0.4 and 7.8 ± 0.2 (Fig. 8*B*). We tentatively ascribe the first transition to Cys-65 and the latter to Cys-68. Both of these values are lower than the typical value of ~8.5–9.0 observed for cysteine, and the data are consistent with the reactivity of both residues toward alkylating reagents (which react with the deprotonated form only). A low pK_a value is normally observed for the N-terminal active site cysteine of thioredoxin-like proteins, which in some cases exhibit pK_a values as low as 3.5 (35). However, the pK_a of the second cysteine is normally estimated to be >9 (32, 36, 37). In this respect, StoA is similar to ResA in that the C-terminal cysteinyl has a pK_a value low enough to be measurable in the stable pH range of the protein.

This large separation of pK_a values is consistent with the close proximity of the two thiol groups, indicating that the ionization of one significantly influences that of the other. The wide separation of active site thiol pK_a values appears to be a general feature of TDORs that act with low specificity (33, 38). For sStoA, we also observed an interdependence of the cysteine acid-base properties: the sStoA single cysteine variants have pK_a values that are very similar, but in the wild-type protein they differ by more than 2 pH units. This suggests that in the wild-type protein Cys-65 and Cys-68 have a significant effect on one another such that the presence of both cysteines causes the pK_a of the N-terminal cysteine to drop, whereas that of C-terminal cysteine rises (relative to the respective single cysteine variants). Such interdependence of pK_a values was not observed for ResA for which respective cysteines in single cysteine variants showed acid-base properties similar to those for the wild-type protein. The stronger interdependence of the cysteine pK_a values in StoA may well be linked to the significantly shorter sulfur-to-sulfur distance observed in reduced StoA (~3.4 Å) compared with that of ResA (~4.5 Å) (12).

Specificity Determinants of StoA and ResA—Here we have demonstrated that StoA and ResA have many features in common. The three-dimensional structure, redox properties, and acid-base properties of active site cysteine residues are similar in these proteins. Furthermore *in vivo*, the two proteins are believed to interact with the same integral membrane protein, CcdA, which functions to supply electrons from thioredoxin (TrxA) in the cytoplasm to the extracytoplasmic compartment (10, 39–41); thus, structural/physical features important for this interaction are expected to be shared by StoA and ResA. Despite the similarities, the two proteins do not exhibit any functional redundancy (2). So how do StoA and ResA achieve specificity for their particular substrates? To try to answer this question, it is important to identify regions of the proteins that do show differences.

First, the two proteins differ in the active site sequence motif: CPPC in StoA and CEPC in ResA. Recently we reported the effects of altering the dipeptide intervening sequence on the properties of ResA, and this included a ResA CPPC variant (21). Significant effects were observed: the redox potential increased by ~25 mV, and the pK_a values of the two cysteines decreased by 1.8 and 1.6 pH units, respectively. These findings are consistent with the midpoint reduction potential and pK_a values measured here for StoA and those previously reported for ResA (13). Alteration of the dipeptide sequence was also shown to impair the *in vivo* activity of ResA (21). Beyond their effect on the biophysical properties of the active site cysteines (*i.e.* redox potential and pK_a values), the intervening two residues may also be important for interaction with potential substrates. The close proximity of these residues to the active site cysteines and the fact that both are exposed on the surface of the protein make it highly likely that they contact partner proteins, at least transiently, and thus affect specificity of interaction.

Second, the protein surfaces close to the active site are subtly different in StoA and ResA. The structures of oxidized and reduced ResA previously revealed redox-linked conformational changes, the most significant of which was the opening up of a hydrophobic cavity close to the active site upon reduction (12). Despite the conservation or conservative substitution of several of the residues that line the ResA cavity, reduction of StoA does not lead to the opening up of an equivalent cavity (see Fig. 9). The lack of a cavity in StoA may be the result of the substitution of Thr-159 (in ResA) with Pro-153 in StoA; Thr-159 undergoes one of the biggest conformational movements upon formation of the hydrophobic cavity in ResA, and thus its replacement by a proline (Pro-153) in StoA might well restrict conformational change in this region of the protein. Alternatively the lack of a cavity in StoA might be linked to the much smaller conformational change in the C*XX*C motif itself, which is likely to be the

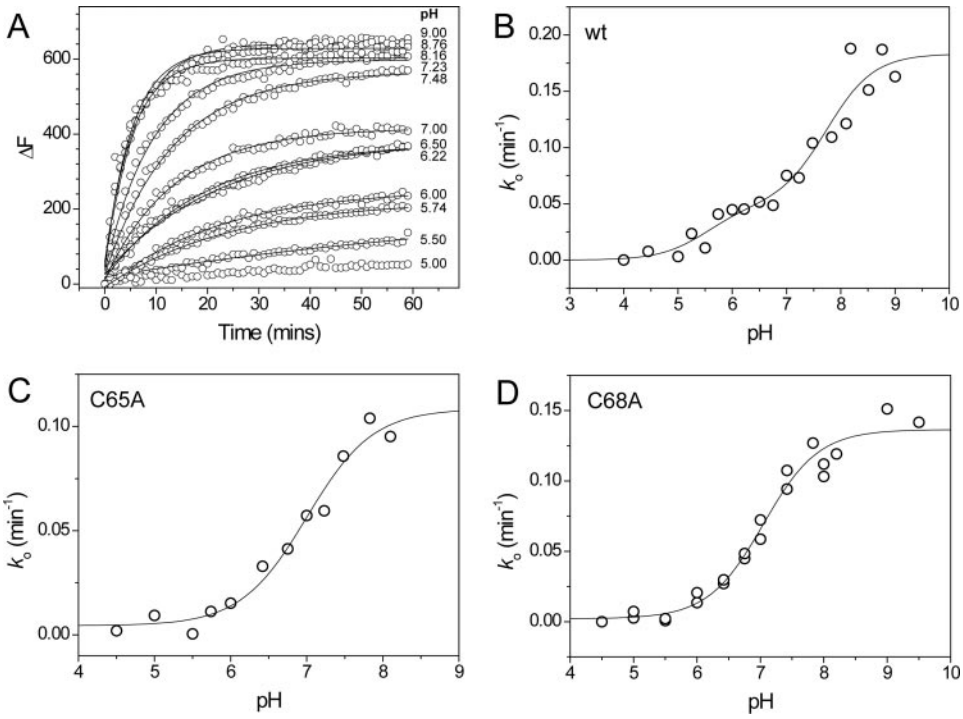

FIGURE 8. **pK_a plots for wild-type and single cysteine sStoA variants.** *A*, time-dependent increases in fluorescence at 510 nm upon reaction of wild-type (*wt*) sStoA (1 μM) with 6-bromoacetyl-2-dimethylaminonaphthalene (15 μM) in PCTC buffer system at pH values from 5 to 9 as indicated at 25 °C. Plots were fitted (*solid lines*) to obtain an observed, pseudo-first order rate constant, k_o. *B*, plot of k_o as a function of pH for wild-type sStoA. The *solid line* shows a fit to supplemental Equation S4. *C* and *D*, plots of k_o as a function of pH obtained from similar experiments with C65A and C68A sStoA, respectively. *Solid lines* represent fits of the data to supplemental Equation S3.

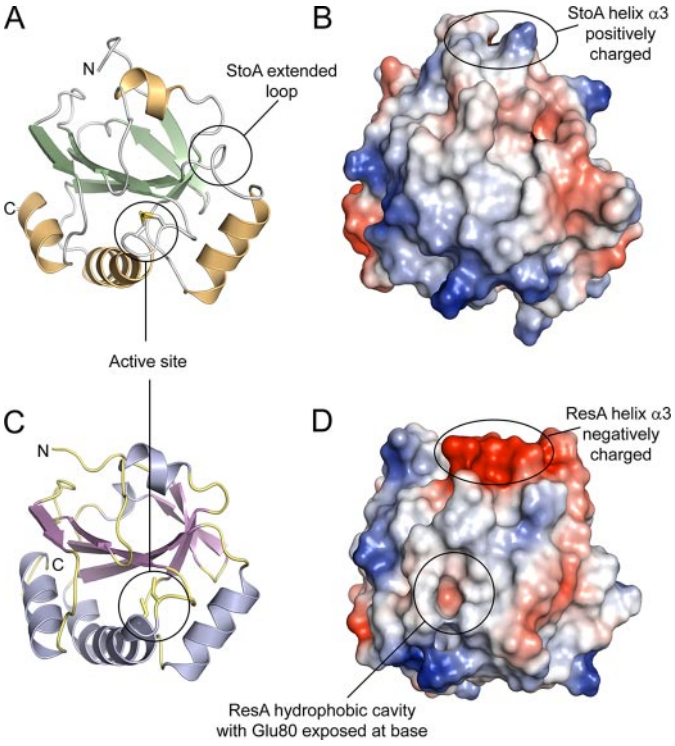

FIGURE 9. **A structural comparison between StoA and ResA.** *A* and *C*, three-dimensional structures of sStoA and sResA, respectively, in schematic representation. *B* and *D*, surface representations of sStoA and sResA, respectively. Regions colored *red* indicate areas of high negative electrostatic potential, whereas *blue* areas indicate areas of high positive potential. Neutral regions are shown in *white*. Electrostatic potentials of surfaces were calculated with PyMOL. The main differences between sStoA and sResA are indicated; see the main text for details.

driving force for the larger conformational changes around the active site motif in ResA.

It has been demonstrated that Glu-80 of ResA plays a key role *in vivo* (14), and *in vitro* studies showed that it is important for the elevated pK_a values of the active site cysteines and that it is capable of hydrogen bonding to amino acid side chain residues bound in the cavity (13, 21). This led us to propose that Glu-80 is important for the binding of apocytochrome substrates to ResA (12–14, 42). This residue is conserved in StoA (Glu-71), and we have shown here that it is also functionally important in StoA (Table 2). Sequence alignments showed that it is conserved in many extracytoplasmic TDORs that are proposed to have a reductive function (13). The data presented here suggest that it fulfils a similar role in ResA and StoA and also in other TDORs. This could be in controlling the acid-base properties of the active site cysteines or through direct participation in the reduction mechanism. Therefore, it is highly unlikely that this glutamate is itself an important determinant for specificity. It remains a possibility that, in ResA, it interacts directly with substrates, but this would be an additional role facilitated by the formation of the hydrophobic cavity upon reduction of the protein. Interaction of Glu-71 with substrate is not favored in StoA because the residue remains buried in both oxidation states.

Third, with the exception of the aforementioned hydrophobic cavity in (reduced) ResA, the only major difference in the electrostatic surfaces of each protein is in helix α3 (StoA numbering), which is positively charged in StoA and negatively charged in ResA (Fig. 9). However, this helix is quite distant from the active site, and it seems unlikely that this feature is responsible for differences in substrate recognition by ResA and StoA.

The final major difference is the presence in StoA of an extended loop between strand β4 and helix α2. In the primary sequence alignment (Fig. 1), this can be clearly seen as an apparent insertion/deletion of several residues that are present in the StoA but not in ResA. The sequence alignment also shows that there is little similarity between the two proteins in this region. The structure shows that the extended β4-α2 loop (composed of Ser-97, Glu-98, Gln-99, and Asn-100) lies close to the active site of StoA (Fig. 9) and represents the most significant difference in the surface shape of StoA compared with ResA and is, therefore, likely to be important for the differential substrate selectivity/specificity of these proteins. For example, this loop could be involved in specific binding interactions with StoA

substrate(s) or could serve to sterically hinder interactions with non-substrate molecules.

Concluding Remarks—The structural, biochemical, and *in vivo* characterization of *B. subtilis* StoA reported here provides new knowledge about this unprecedented endospore biogenesis factor whose physiological function is not completely understood (9). Furthermore the data reveal that this low potential extracytoplasmic TDOR is remarkably similar to ResA, another well characterized extracytoplasmic TDOR from the same organism that is required for cytochrome *c* maturation. It is thought that both proteins interact with the same integral membrane protein, CcdA, which supplies them with electrons from the cytoplasm. The high structural similarity of ResA and StoA is no doubt connected with their shared need to interact with this protein. Despite the large extent of their similarity (in both sequence and structure), the proteins cannot functionally substitute for one another *in vivo*. Bacteria usually contain several thioredoxin-like proteins, soluble in the cytoplasm as well as membrane-bound. *B. subtilis* contains at least 10 such proteins, and none of these are essential for growth, indicating a narrow substrate specificity for each protein (43). The results of this work raise important general questions about how TDORs achieve substrate specificity: ResA can recognize at least four different apo-*c*-type cytochrome polypeptides as substrates, whereas StoA recognizes a different but as yet unknown substrate(s) critical for endospore cortex biosynthesis. From the structures of StoA and ResA, we have identified four principal structural differences between the two proteins that we believe provide the basis of substrate specificity/selectivity. The work demonstrates that protein-substrate specificity/selectivity can apparently be achieved through remarkably subtle variations in amino acid sequence and three-dimensional structure.

Acknowledgments—We thank Ingrid Stål for technical assistance, Dr. Allison Lewin for assistance with redox and pK_a measurements, Dr. Marit Lenman for transporting a critical sample, and beam line staff at the European Synchrotron Radiation Facility for assistance in x-ray data collection.

REFERENCES

1. Piggot, P. J., and Hilbert, D. W. (2004) *Curr. Opin. Microbiol.* **7,** 579–586
2. Erlendsson, L. S., Möller, M., and Hederstedt, L. (2004) *J. Bacteriol.* **186,** 6230–6238
3. Imamura, D., Kobayashi, K., Sekiguchi, J., Ogasawara, N., Takeuchi, M., and Sato, T. (2004) *J. Bacteriol.* **186,** 5450–5459
4. Raina, S., and Missiakas, D. (1997) *Annu. Rev. Microbiol.* **51,** 179–202
5. Dailey, F. E., and Berg, H. C. (1993) *Proc. Natl. Acad. Sci. U. S. A.* **90,** 1043–1047
6. Meima, R., Eschevins, C., Fillinger, S., Bolhuis, A., Hamoen, L. W., Dorenbos, R., Quax, W. J., van Dijl, J. M., Provvedi, R., Chen, I., Dubnau, D., and Bron, S. (2002) *J. Biol. Chem.* **277,** 6994–7001
7. Yamanaka, H., Kameyama, M., Baba, T., Fujii, Y., and Okamoto, K. (1994) *J. Bacteriol.* **176,** 2906–2913
8. Kadokura, H., Katzen, F., and Beckwith, J. (2003) *Annu. Rev. Biochem.* **72,** 111–135
9. Möller, M., and Hederstedt, L. (2006) *Antioxid. Redox Signal.* **8,** 823–833
10. Carlsson Möller, M., and Hederstedt, L. (2008) *J. Bacteriol.* **190,** 4660–4665
11. Erlendsson, L. S., Acheson, R. M., Hederstedt, L., and Le Brun, N. E. (2003) *J. Biol. Chem.* **278,** 17852–17858
12. Crow, A., Acheson, R. M., Le Brun, N. E., and Oubrie, A. (2004) *J. Biol. Chem.* **279,** 23654–23660
13. Lewin, A., Crow, A., Oubrie, A., and Le Brun, N. E. (2006) *J. Biol. Chem.* **281,** 35467–35477
14. Hodson, C. T. C., Lewin, A., Hederstedt, L., and Le Brun, N. E. (2008) *J. Bacteriol.* **190,** 4697–4705
15. Fortnagel, P., and Freese, E. (1968) *J. Bacteriol.* **95,** 1431–1438
16. Potterton, L., McNicholas, S., Krissinel, E., Gruber, J., Cowtan, K., Emsley, P., Murshudov, G. N., Cohen, S., Perrakis, A., and Noble, M. (2004) *Acta Crystallogr. Sect. D Biol. Crystallogr.* **60,** 2288–2294
17. Adams, P. D., Grosse-Kunstleve, R. W., Hung, L. W., Ioerger, T. R., McCoy, A. J., Moriarty, N. W., Read, R. J., Sacchettini, J. C., Sauter, N. K., and Terwilliger, T. C. (2002) *Acta Crystallogr. Sect. D Biol. Crystallogr.* **58,** 1948–1954
18. Leslie, A. G. (2006) *Acta Crystallogr. Sect. D Biol. Crystallogr.* **62,** 48–57
19. Evans, P. (2006) *Acta Crystallogr. Sect. D Biol. Crystallogr.* **62,** 72–82
20. Murshudov, G. N., Vagin, A. A., and Dodson, E. J. (1997) *Acta Crystallogr. Sect. D Biol. Crystallogr.* **53,** 240–255
21. Lewin, A., Crow, A., Hodson, C. T. C., Hederstedt, L., and Le Brun, N. E. (2008) *Biochem. J.* **414,** 81–91
22. Schägger, H., and von Jagow, G. (1987) *Anal. Biochem.* **166,** 368–379
23. Marmur, J. (1961) *J. Mol. Biol.* **3,** 208–218
24. Hanahan, D., Jessee, J., and Bloom, F. R. (1991) *Methods Enzymol.* **204,** 63–113
25. Pace, C. N., Vajdos, F., Fee, L., Grimsley, G., and Gray, T. (1995) *Protein Sci.* **4,** 2411–2423
26. Edeling, M. A., Guddat, L. W., Fabianek, R. A., Thony-Meyer, L., and Martin, J. L. (2002) *Structure* (*Lond.*) **10,** 973–979
27. Ouyang, N., Gao, Y. G., Hu, H. Y., and Xia, Z. X. (2006) *Protein Struct. Func. Bioinformat.* **65,** 1021–1031
28. Goulding, C. W., Apostol, M. I., Gleiter, S., Parseghian, A., Bardwell, J., Gennaro, M., and Eisenberg, D. (2004) *J. Biol. Chem.* **279,** 3516–3524
29. Kortemme, T., and Creighton, T. E. (1995) *J. Mol. Biol.* **253,** 799–812
30. Krause, G., Lundstrom, J., Barea, J. L., Delacuesta, C. P., and Holmgren, A. (1991) *J. Biol. Chem.* **266,** 9494–9500
31. Lin, T. Y., and Kim, P. S. (1989) *Biochemistry* **28,** 5282–5287
32. Kallis, G. B., and Holmgren, A. (1980) *J. Biol. Chem.* **255,** 261–265
33. Nelson, J. W., and Creighton, T. E. (1994) *Biochemistry* **33,** 5974–5983
34. Haugland, R. P., Johnson, I. D., Spence, M. T. Z., and Basey, A. (2005) *Handbook: a Guide to Fluorescent Probes and Labeling Technologies*, 10th Ed., Chapter 2, Invitrogen Corp., Carlsbad, CA
35. Huber-Wunderlich, M., and Glockshuber, R. (1998) *Fold. Des.* **3,** 161–171
36. Chivers, P. T., Prehoda, K. E., Volkman, B. F., Kim, B. M., Markley, J. L., and Raines, R. T. (1997) *Biochemistry* **36,** 14985–14991
37. Jeng, M. F., Holmgren, A., and Dyson, H. J. (1995) *Biochemistry* **34,** 10101–10105
38. Nordstrand, K., Aslund, F., Meunier, S., Holmgren, A., Otting, G., and Berndt, K. D. (1999) *FEBS Lett.* **449,** 196–200
39. Schiött, T., and Hederstedt, L. (2000) *J. Bacteriol.* **182,** 2845–2854
40. Schiött, T., Throne-Holst, M., and Hederstedt, L. (1997) *J. Bacteriol.* **179,** 4523–4529
41. Schiött, T., von Wachenfeldt, C., and Hederstedt, L. (1997) *J. Bacteriol.* **179,** 1962–1973
42. Crow, A., Le Brun, N. E., and Oubrie, A. (2005) *Biochem. Soc. Trans.* **33,** 149–151
43. Smits, W. K., Dubois, J. Y. F., Bron, S., van Dijl, J. M., and Kuipers, O. P. (2005) *J. Bacteriol.* **187,** 3921–3930
44. DeLano, W. L. (2002) *The PyMOL Molecular Graphics System*, DeLano Scientific, San Carlos, CA
45. Amann, E., Brosius, J., and Ptashne, M. (1983) *Gene* (*Amst.*) **25,** 167–178
46. Stragier, P., Bonamy, C., and Karmazyncampelli, C. (1988) *Cell* **52,** 697–704